FERMILAB-PUB-09-034-APC

Physics design of front ends for superconduting ion linacs

P. N. Ostroumov
Argonne National Laboratory, Argonne, Illinois 60439 USA

J.-P. Carneiro*
Fermi National Accelerator Laboratory, Batavia, Illinois 60510 USA
(Dated: January 30, 2009)

Superconducting (SC) technology is the only option for CW linacs and is also an attractive option for pulsed linacs. SC cavities are routinely used for proton and H^- beam acceleration above 185 MeV. Successful development of SC cavities covering the lower velocity range (down to 0.03c) is a very strong basis for the application of SC structures in the front ends of high energy linacs. Lattice design and related high-intensity beam physics issues in a ∼400 MeV linac that uses SC cavities will be presented in this talk. In particular, axially-symmetric focusing by SC solenoids provides strong control of beam space-charge and a compact focusing lattice. As an example, we discuss the SC front-end of the H^- linac for the FNAL Proton Driver.

PACS numbers: 29.27.-a,41.75.Cn

I. INTRODUCTION

High-intensity proton accelerators based on superconducting (SC) linacs have experienced a spectacular development over the last decade [1]. These proton drivers can deliver up to multi-MW beams in either CW or pulsed mode (<100 Hz) and are being developed for applications such as spallation neutron sources, production of radioactive ion beams (RIB), transmutation of nuclear waste or neutrino physics. Typical kinetic energies for such linacs range from 40 MeV to 8 GeV. Due to the RF power consumption, high duty factor or CW operation of high power accelerators is inconceivable with Normal Conducting (NC) cavities and SC technology becomes the natural choice. Examples for CW ion drivers based on SC linacs are the heavy-ion linac ATLAS operated at Argonne national Laboratory (ANL) [2] or the multi-user facility SARAF [3] being constructed in Israel which is expected to deliver in 2010 deuteron beams with an energy of 40 MeV at 80 kW beam power. The proposed RIB facilities AEBL [4] and EURISOL [5] aim at delivering ion beams at an energy of respectively >200 MeV/u and 1 GeV for a corresponding beam power of 400 kW and 5 MW. The development of SC cavities for $\beta < 1$ gave rise in the recent years to several SC pulsed proton drivers. The Spallation Neutron Source accelerator (SNS, [6]) at Oak Ridge is, as of today, the only pulsed SC proton driver in operation. Its final goal is to deliver a proton beam of 1.0 GeV and 1.4 MW at a repetition rate of 60 Hz for neutron scattering research. Several other pulsed SC proton drivers are under development for neutron production like the Japan Proton Accelerator Research Complex linac [7] (J-PARC, 1.3 GeV, 10 MW, 50 Hz) or for neutrino physics like the CERN Superconducting Proton Linac [8] (SPL, 5 GeV, 4 MW, 50 Hz) or the FNAL Proton Driver [9].

The proposed FNAL Proton Driver is an 8-GeV SC H^- linac designed to deliver $1.56 \cdot 10^{14}$ protons to the Main Injector in typical pulse lengths of 1 msec leading to an average beam current of 25 mA per pulse. At a kinetic energy of 8 GeV and a repetition rate of 10 Hz the corresponding beam average power is ∼2 MW. This paper describes the physics design of the FNAL 8-GeV linac SC front-end (∼420 MeV). A detailed description of the full linac is presented in Reference [10].

II. FRONT END DESIGN

The main concern in the design of the FNAL 8-GeV linac (as for any high-intensity proton linac) is the control of the beam losses at a level that allows "hands-on maintenance". Experience on the LANSCE accelerator at Los Alamos has lead the accelerator community to take as a rule of thumb that "hands-on maintenance" is possible if uncontrolled losses along the linac are kept below 1 W/m. For the FNAL 8-GeV linac operating at 2 MW, this means a relative loss of only $5 \cdot 10^{-7}$ particle per meter. As a consequence, particular attention has been taken in the design of the front-end of the linac to control the growth of beam halo that would lead to particle losses.

A. Why Spoke Resonators ?

Typical front-end designs for proton drivers are made of NC structures (like Drift Tube Linac and Coupled Cavity Linac) with a transition to SC ones at high energy: 160 MeV for SPL, 185 MeV for SNS or 400 MeV for J-PARC. An original approach has been taken for the design of the front-end of the FNAL 8-GeV linac. Taking advantage of the development and excellent performance of spoke cavities ([11], [12]) it was decided to make

*Corresponding author. Electronic address: carneiro@fnal.gov

a transition from NC to SC structures at low energy. From ∼10 MeV to ∼420 MeV the beam will be accelerated with SC Single Spoke Resonators and SC Triple Spoke Resonators. Compared to standard NC accelerating structures, the SC cavities offer higher accelerating gradients and cost-effective operation. Furthermore, the use of high-power ferrite vector modulators [13] allows the fan-out of RF power from a klystron to feed multiple cavities. With this outstanding feature of the FNAL 8-GeV linac, only five J-PARC type 2.5 MW klystrons are necessary to power the 420-MeV front-end of the linac while, for instance, the SNS 185-MeV front-end requires 11 klystrons.

B. Why Superconduting Solenoid ?

SC solenoids have been selected as the focusing elements for the front-end (up to ∼120 MeV limited by H^- stripping) of the FNAL 8-GeV linac in lieu of the standard quadrupole structures.

The idea of using SC solenoids in the front-end of high-intensity SC proton linacs was discussed conceptually by Garnett [14]. Our design differs from [14] by efficient use of the available voltage from SC cavities and provides much higher real-estate gradients tighter with better control of space-charge by reduced length of the focusing periods.

Several advantages arise from the use of SC solenoids:

- to provide stability for all particles inside the separatrix the defocusing factor

$$\gamma_s = \frac{\pi}{2}\frac{1}{(\beta\gamma)^3}\frac{L_f^2}{\lambda}\frac{eE_m\sin(\phi_s)}{m_0c^2} \tag{1}$$

  should be kept below ∼ 0.7. SC solenoids shorten the length of the focusing period (by a factor of 2 compared to FODO focusing) which facilitates the use of the higher accelerating gradients offered by the SC cavities. In Eq. 1 : m_0c^2 is the particle rest energy, β is the particle relative velocity, γ is the Lorentz factor, λ is the wavelength of the RF field, L_f is the length of the focusing period, E_m is the amplitude of the equivalent traveling wave of the accelerating field and ϕ_s is the synchronous phase

- the smooth axial-symmetric focusing provided by SC solenoids in the MEBT mitigates the formation of halo which can take place with weak asymmetric focusing as observed at SNS [15]

- as discussed in [16], lattices using SC solenoids are less sensitive to misalignments, errors and beam mismatches.

  Furthermore, SC solenoids are perfectly suitable for SC environment with SRF. SC solenoids are easily re-tunable to adjust to the accelerating gradient variation from cavity to cavity and can they can also be supplemented with dipole coils for corrective steering of the beam centroid. SC solenoids have been used at ATLAS facility for several decades [2] and implemented in new facilities such as ISAC-II [17] and SARAF [3].

C. FNAL Proton Driver front-end lattice

A schematic layout of the front-end of the FNAL 8-GeV linac is presented in Figure 1. The different sections of the linac with corresponding main parameters are presented in Table 1. The linac front-end is made of 73 focusing periods with lengths varying from 49 cm to 3.8 m. The H^- beam from the Ion Source is bunched and accelerated up to 2.5 MeV by a 325 MHz RFQ. At that energy the MEBT section provides space for a fast beam chopper (<2 ns) that eliminates unwanted bunches and forms an optimal beam time structure for injection into the Main Injector. This chopping decreases the beam average current over the 1 msec pulse from ∼45 mA to ∼25 mA. Acceleration from 2.5 MeV to 10 MeV is provided by 16 room temperature cross-bar H-type (CH) cavities. The CH cavities, foreseen for the future proton synchrotron of GSI [18], present very high shunt impedance (90 MOhm/m to 60 MOhm/m) and are an excellent option. The use of SC technology is not appropriate for this energy range as it would require time-consuming and expensive development of multiple SC designs. Above 10 MeV, SC RF structures are used. Two types of Single Spoke Resonators and one type of Triple Spoke Resonator (SSR1, SSR2 and TSR) accelerate the beam up to ∼420 MeV. At this energy, spoke cavities become less efficient and the beam is further accelerated up to 8 GeV using Squeezed ILC ($\beta_g = 0.81$) and ILC ($\beta_g = 1$) 1.3 GHz cavities. The frequency transition at 420 MeV is favorable to longitudinal beam dynamics [10].

III. EMITTANCE DEFINITION

In this paper the RMS normalized transverse emittance is defined by the relation [19] :

$$\epsilon_u = \beta\gamma\sqrt{\langle u^2\rangle\langle (u')^2\rangle - \langle uu'\rangle^2} \tag{2}$$

with β the beam relative velocity, γ the Lorentz factor, u and u' the transverse coordinate and divergence of x or y, and $\langle\rangle$ an RMS value. In the longitudinal plane, the RMS normalized emittance takes the form:

$$\epsilon_z = \frac{1}{m_0c^2}\sqrt{\langle (\delta z)^2\rangle\langle (\delta p_z)^2\rangle - \langle \delta_z\delta p_z\rangle^2} \tag{3}$$

with m_0c^2 the particle rest mass, δz and δp_z the difference of the particle coordinates from the beam's aver-

FIG. 1: Schematic layout of the front-end of the FNAL 8-GeV Superconducting Linac.

TABLE I: Main parameters for each section of the front-end linac with focusing type (S: Solenoid, R: Resonator, nR: n Resonators, F: Focusing quad, D: Defocusing quad and L_f: Period length).

Section Name	W_{out} (MeV)	Cavities No.	Focusing Type	Period No.	L_f (m)	z (m)
RFQ	2.5	1	-	-	-	4
MEBT	2.5	2	S1R	-	-	6.65
CH	10	16	S1R	16	0.49-0.75	17
SSR1	32	18	S1R	18	0.75	31.4
SSR2	124	33	S2R	18	1.6	61.0
TSR	421	42	FRDR	21	3.8	142.2
Total	∼421	112		73		∼142.2

age position and momentum. Concerning the total emittance, this quantity is defined in this paper as the area of the ellipse in the transverse and longitudinal trace space containing the desired fraction of the beam.

IV. FRONT END SIMULATIONS AT 45 mA

The main tool used for the design of the FNAL 8-GeV linac is the beam dynamics code TRACK [20]. For benchmarking purposes, the simulations have also been performed with the code ASTRA [21] developed by DESY. Mainly used for the design of electron photo-injectors, it offers also the possibility of simulating hydrogen ion beams. Both codes handle 3D space-charge. Benchmarking starts at the RFQ exit since ASTRA does not cover RFQ beam dynamics. Simulations presented in this section are based on $2 \cdot 10^5$ macro-particles in both codes and a 3D equidistant Cartesian grid of $129 \times 129 \times 257$ and $129 \times 129 \times 129$ mesh points respectively in `TRACK` and `ASTRA` for the space-charge calculations.

A. The Radio Frequency Quadrupole

The FNAL RFQ is ∼3 m long and is capable of efficiently accelerating bunch beam currents up to 140 mA. The RFQ physics design and beam dynamics simulations were presented elsewhere [22]. One original point in the design of the RFQ is the use of an output radial matcher to produce axially-symmetric beam. Particular attention was taken to preserve transverse emittance and to minimize the longitudinal emittance while maximizing the accelerating rate.

B. Lattice Design

The design of the FNAL 8-GeV linac has been performed following the general design requirements for high-intensity proton linacs [10] necessary to minimize RMS emittance growth along the linac:

- keep the zero current phase advance per focusing period in all planes below 90° to avoid parametrically-excited instabilities at high current

- provide smooth evolution of the wavenumbers (k_{T0}, and k_{L0}) of both transverse and longitudinal oscillations along the linac. This feature minimizes the potential for mismatch and helps assure a current independent lattice. The wavenumbers of particle oscillations are expressed as

$$k_{T0} = \frac{\sigma_{T0}}{L_f}, \qquad k_{L0} = \frac{\sigma_{L0}}{L_f} \tag{4}$$

  where σ_{T0}, and σ_{L0} are the transverse and longitudinal phase advance per focusing period of length L_f at zero current

- avoid the n=1 parametric resonance between the transverse and longitudinal motion. The condition for occurrence of an n-th order parametric resonance of transverse motion to occur is

$$\sigma_{T0} = \frac{n}{2}\sigma_{L0} \tag{5}$$

The strongest resonance is for n=1 and can occur particularly in SC linacs due to the availability of high accelerating gradients and relatively long focusing periods. It can be avoided by properly choosing the linac operation tunes in the Kapchinskiy stability diagram

- avoid strong space-charge resonances by selecting stable areas in the Hofmann's stability charts or use fast resonance crossing
- maintain beam equipartitioning to avoid energy exchange between the transverse and longitudinal planes that can occur via space-charge forces

For NC linacs all the above listed requirements can be fulfilled with peak currents up to ∼150 mA as presented in reference [23]. Cost-effective SC linacs are more challenging for satisfying these specifications. For example, cavities and focusing elements in SC linacs are located in relatively long cryostats with inevitable drift spaces between them. Also, the focusing period lengths can present a sharp change at transitions between linac sections with different types of cavities.

C. Zero current

Figure 2 presents TRACK and ASTRA simulations of the FNAL 8-GeV linac font-end linac at zero current. The variation of the transverse and longitudinal phase advance along the linac is presented in Figure 2(a). The observable, but insignificant, difference between the phase advances from TRACK and ASTRA comes primarily from the different technique of calculation of the phase advances. Due to the changing length of the focusing period at transitions between different types of SC cavities, the phase advances present strong but innocuous jumps. Apart from few periods, the phase advances remain below 90°. Figure 2(b) shows the smooth change of the transverse and longitudinal wavenumbers along the linac. The smooth evolution of the transverse wavenumber is provided by selecting the appropriate length of the focusing periods (as shown in Table 1) and focusing field strengths. Concerning the longitudinal wavenumber, smooth evolution is obtained by properly adjusting the synchronous phase of each cavity. The Kapchinskiy stability diagram (Fig. 2(c)) presents the evolution of $\cos(\sigma_{T0})$ as a function of the defocusing factor γ_s (Eq. 1). The gray area corresponds to the n=1 parametric resonance and the dashed line corresponds to the stability required for the particles near the separatrix boundary at a phase angle of $-2|\phi_s|$. The majority of the 73 period tune points are located in the stable areas of the Kapchinskiy diagram. The few tune points located outside the stability region correspond to the first focusing periods of the CH section. These regions present essentially no problem since the instability takes place over a short distance compared to the betatron oscillation wavelengths.

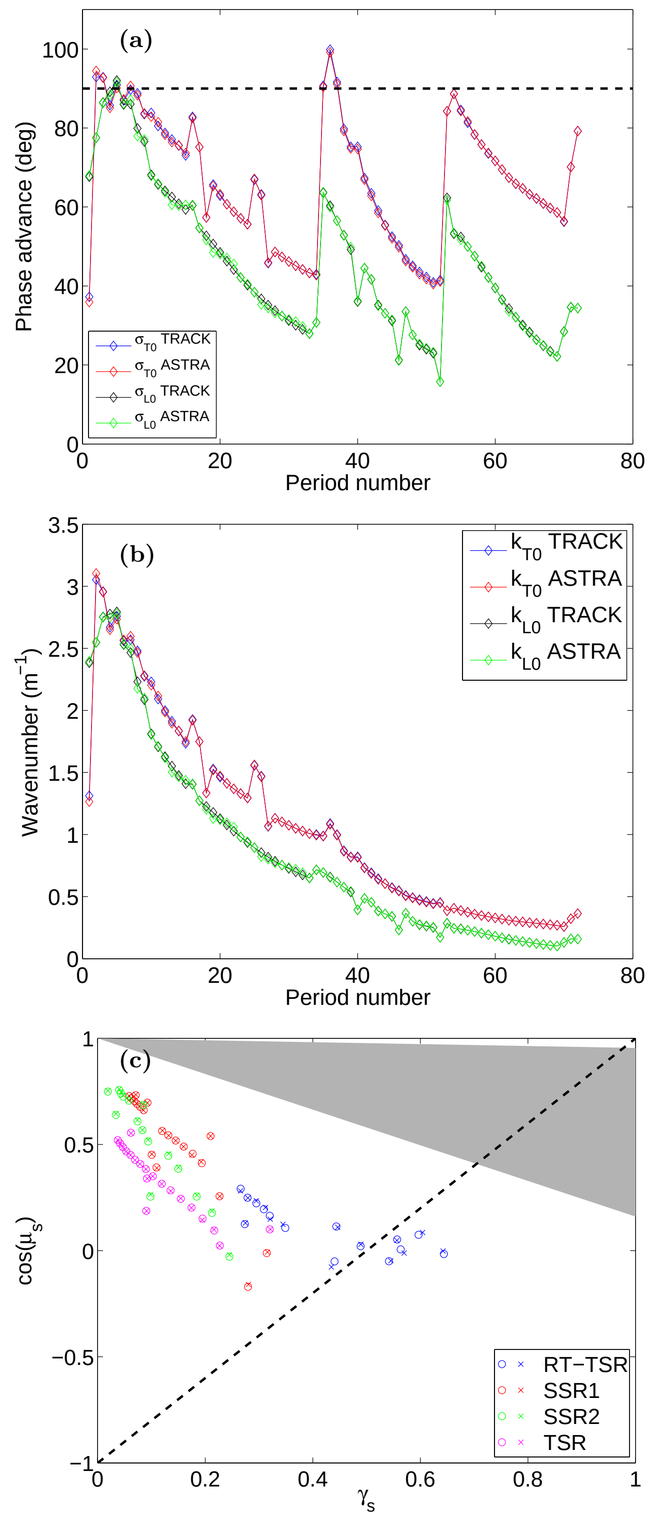

FIG. 2: `TRACK` and `ASTRA` simulations of the FNAL 8-GeV linac front-end at zero current : (a) transverse and longitudinal phase advances, (b) transverse and longitudinal wavenumbers and (c) Kapchinskiy stability diagram. The gray area in (c) shows the boundary of the n=1 parametric resonance and the dashed line particle located near the separatrix. In (c) circles represent `TRACK` and crosses `ASTRA`.

.

D. Tune depression and stability chart

The tune depression is an important parameter to monitor in the design of an high intensity accelerator since not only it is a useful tool to quantity the parametric resonances [24] between the single particles of the beam and the core of the beam, it also gives informations about coherent resonances of the core of the beam with itself called the core-core resonances [25]. While the former resonances are related to halo formation the later are related to issue of equipartition.

The tune depression η is defined by the relation :

$$\eta = \frac{k}{k_0} \tag{6}$$

where k is the wavenumber per focusing period depressed by the space-charge and k_0 the same parameter without space-charge. The transverse and longitudinal tune depression computed with `TRACK` and `ASTRA` for each section of the linac front-end at the design current of 45 mA are reported respectively in Fig. 3(a) and Fig. 3(b). The tune depression displayed in these figures has been computed following the general equation described in Reference [26] which in the transverse plane takes the form :

$$\eta_T^2 = 1 - \frac{3qI\lambda(1-f)}{4\pi\epsilon_0 m_0 c^3\gamma^3\beta^2(r_x+r_y)r_x r_z}\left(\frac{1}{k_{T0}}\right)^2 \tag{7}$$

and in the longitudinal one:

$$\eta_L^2 = 1 - \frac{3qI\lambda f}{4\pi\epsilon_0 m_0 c^3\gamma^3\beta^2(r_x r_y r_z)}\left(\frac{1}{k_{L0}}\right)^2 \tag{8}$$

with I the average current over an RF period, r_x, r_y and r_z the semiaxis of the equivalent ellipse over the focusing period length related to the RMS beam sizes σ_i by $r_i = \sqrt{5}\cdot\sigma_i$, $i = x, y, z$, f the corresponding ellipsoid form factor and all other parameters being previously defined. Figures 3(a) and 3(b) predict a moderate transverse and longitudinal tune depression ($0.5 < \eta_{T,L} < 1.0$). Some points do present stronger but inoffensive tune depression (< 0.5) due to the matching between the different sections of the front-end linac.

If the beam presents a certain combination of anisotropy, tune depression and tune ratio it can experience emittance exchange between the transverse and longitudinal planes. This effect, known as equipartitioning, is due to the collective space-charge density oscillations of the beam. A commonly used tool to monitor these core-core resonances is the Hofmann's stability chart [27] which indicates, for a given transverse-to-longitudinal emittance ratio, regions sufficiently large to ensure a stable operation of nonequipartitioned beam. Figure 3(c) presents the Hofmann's stability chart for

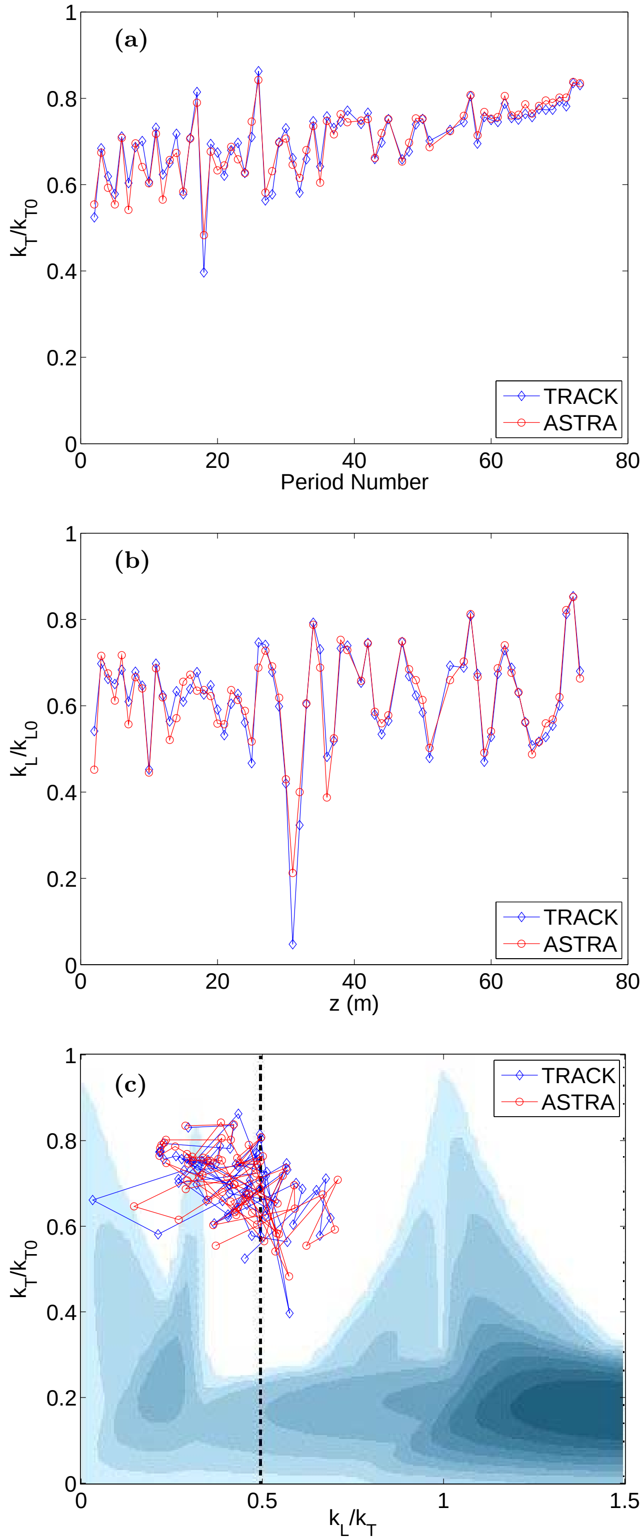

FIG. 3: (a) Transverse and (b) Longitudinal tune depression per front-end linac focusing period and (c) corresponding Hofmann's stability chart for a longitudinal to transverse emittance ratio of ϵ_L/ϵ_T=2 and a linac design current of 45 mA. Tunes are from `TRACK` and `ASTRA`.

.

the FNAL 8-GeV linac front-end at the design current of 45 mA and for a longitudinal to transverse emittance ratio of $\epsilon_L/\epsilon_T = 2$. The horizontal axis on the chart is the ratio between the transverse and longitudinal tune depression and the vertical is the tune depression. The shaded areas indicate regions where nonequipartitioned beams are subject to space-charge coupling resonances that are expected to cause emittance transfer. The dangerous resonance in the chart is the 4-th order even mode one located around a tune ratio of 1. The peaks on the left represent weak coupling resonances that would take a long time to develop. As depicted in Fig. 3(c), the operating tunes computed with TRACK and ASTRA lie in stable (white) areas. Therefore space-charge driven resonances are not a concern for the current design of the FNAL 8-GeV linac front-end.

E. Emittance growth and beam losses

Figure 4 shows simulated transverse and longitudinal emittance growth for the FNAL 8-GeV linac front-end which is at an acceptable level and is mainly due to imperfection matching at the lattice transitions. In fact, the beam mismatch causes envelope oscillations leading to a larger but acceptable emittance growth [22]. A detailed beam loss analysis of the full linac reported in [28] using TRACK shows that the actual design indicates very limited losses for typical misalignments and RF errors. The use of SC cavities with large aperture enables the ratio aperture-to-RMS-beam-size to stay higher than 10 in most of the linac, a safe margin to avoid losses as discussed in [29].

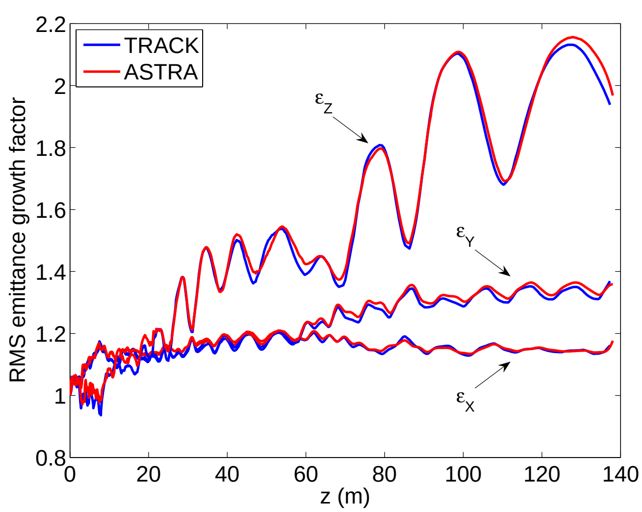

FIG. 4: RMS transverse and longitudinal emittance growth factor in the FNAL 8-GeV linac front-end at 45 mA. From `TRACK` and `ASTRA` with $2 \cdot 10^5$ macro-particles.

V. FRONT END SIMULATIONS AT 100 mA

The front-end design developed for the FNAL 8-GeV linac can be successfully applied for acceleration of 100 mA proton/H$^-$ beams. As was shown by LANL during the work on several projects [30], for high-intensity beams above ∼100 mA it is reasonable to use an RFQ up to ∼7 MeV. Below we discuss a front-end based on the FNAL 8-GeV linac lattice but with a 7 MeV RFQ. A schematic layout of the front-end at 100 mA is presented in Figure 5. For the purpose of beam dynamics simulations we assume that perfect 6D matching is provided at the entrance of the linac at 7 MeV. The lattice beyond 7 MeV is the same as in the FNAL 8-GeV linac with slightly different geometrical beta of SSR1 and SSR2 for better matching to beam velocity.

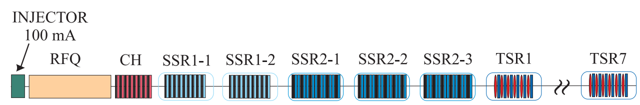

FIG. 5: Possible layout of the front-end at 100 mA.

Tracking of the 100 mA distribution has been performed with `TRACK` using $2 \cdot 10^5$ macro-particles and a grid of 65 × 65 × 129 mesh points for the 3D space-charge routine. Figure 6 shows a reasonable emittance growth factor in all three planes of the 100 mA beam. As mentioned in the previous section, the primary effect for the observed RMS emittance growth is attributed to imperfect matching between the different transitions of the linac.

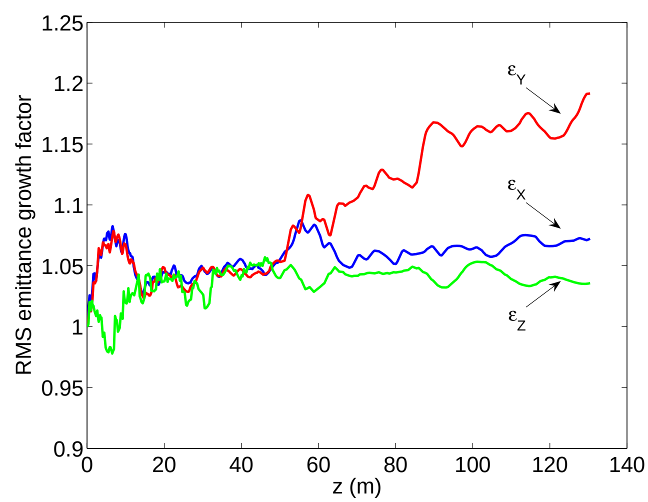

FIG. 6: `TRACK` simulations of the RMS emittance growth factor in the front-end from 7 MeV to 420 MeV at 100 mA.

Evolution of the RMS and maximum beam envelope and bunch length is presented in Figure 7. These simulations indicate that the maximum halo production is limited to ∼5 times its RMS value in all three planes, a

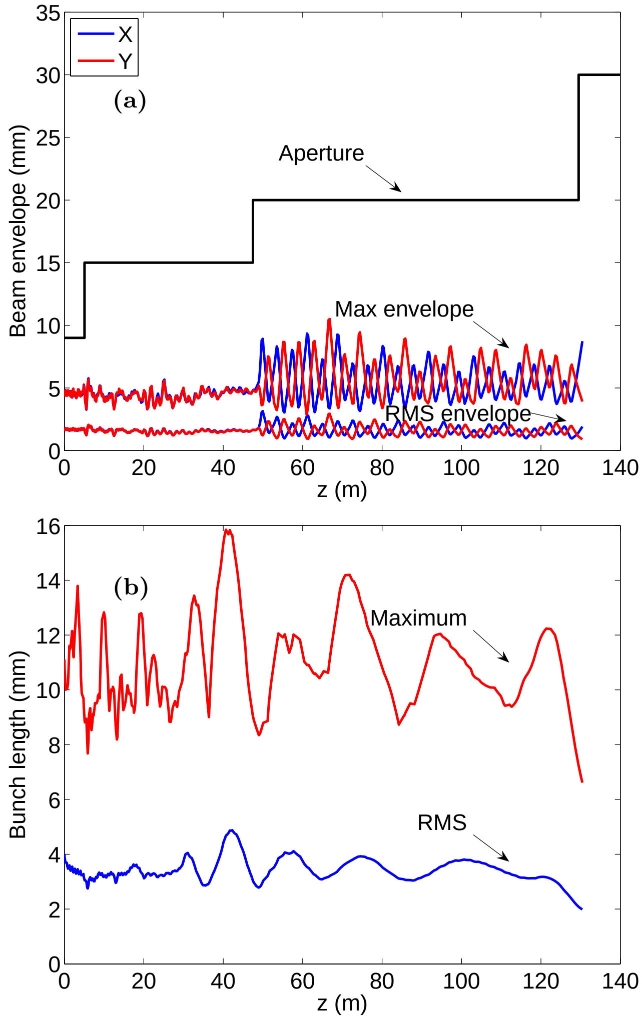

FIG. 7: TRACK simulations of the front-end from 7 MeV to 420 MeV at 100 mA: (a) RMS and Maximum beam envelopes and (b) RMS and Maximum bunch length.

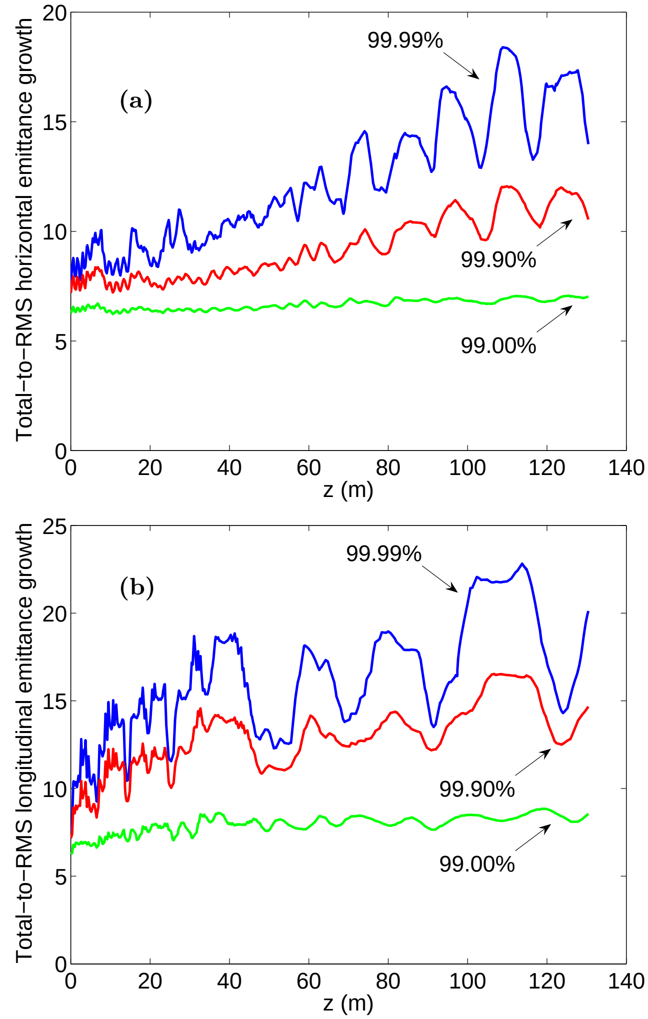

FIG. 8: TRACK simulations of the Total-to-RMS emittance ratio (99.99%, 99.9% and 99%) in the front-end from 7 MeV to 420 MeV at 100 mA: (a) horizontal (b) longitudinal.

reasonable value according to [29]. Furthermore, the use of SC resonators with large aperture (see Fig. 7) enables the ratio between the minimum beam tube radius and the RMS beam size to stay higher than 10, a safe margin to avoid losses as discussed in Section IV E.

The total-to-RMS emittance ratio relates to the tail of the distribution and indicates how far particles deviate in the phase-space compared to the core of the distribution [31]. This ratio is therefore a useful tool to monitor halo formation. Figure 8 shows the evolution of the 99.99%, 99.90% and 99% horizontal and longitudinal total-to-RMS emittance ratio along the linac front-end. A rather constant evolution of the 99% horizontal and longitudinal emittance ratio is presented in Figures 8(a) and 8(b) respectively. A significant increase of the 99.9% and 99.99% emittance ratio is visible in both the horizontal and longitudinal planes and can be related to the imperfect matching between the different sections. For the present preliminary studies of the linac front-end operating at 100 mA, it is noteworthy that only 0.1% of the particles are outside $\sim$15$\cdot$ ϵ_{RMS}. This represents an acceptable level and enables the transport of the $2 \cdot 10^5$ beam distribution in the linac front-end without any losses.

Figure 9 presents the Hofmann's stability charts for two configurations of the linac front-end: the first chart (Fig. 9(a)) corresponds to a longitudinal to transverse emittance ratio of $\epsilon_L/\epsilon_T = 3$ which has been considered up to now (Fig. 6 to Fig. 8) and the second chart (Fig. 9(b)) corresponds to a longitudinal to transverse emittance ratio of $\epsilon_L/\epsilon_T = 2$. The computation of the tunes presented in Figure 9 has been performed following the indications presented in Section IV D. As observed in Figure 9(a), the operating tunes computed with TRACK in the case of $\epsilon_L/\epsilon_T = 3$ lie in stable areas. The same conclusion cannot by drawn for the emittance ratio of $\epsilon_L/\epsilon_T = 2$. In fact, in Fig. 9(b) many operating tunes hit

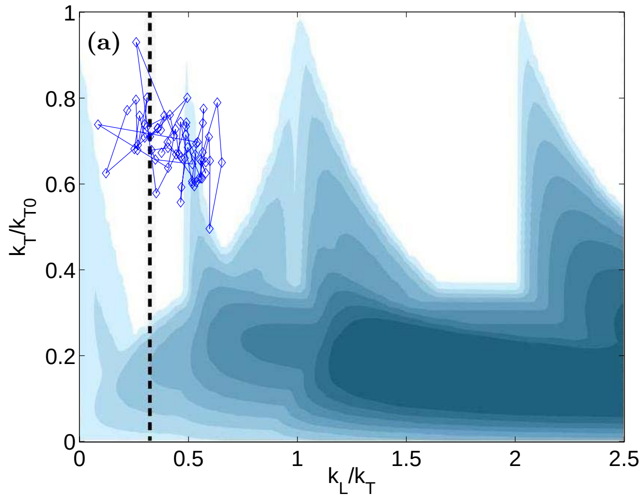

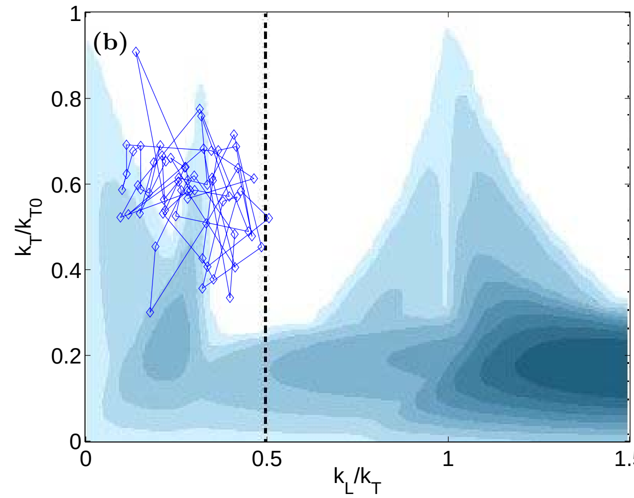

FIG. 9: Hofmann's stability charts for the front-end from 7 MeV to 420 MeV at 100 mA and two configurations: initial longitudinal to transverse emittance ratio of (a) ϵ_L/ϵ_T=3 and (b) ϵ_L/ϵ_T=2. From TRACK.

the resonances. We also observed for this case an RMS emittance growth approximately twice stronger than the one reported in Fig. 6 for the case $\epsilon_L/\epsilon_T = 3$.

We conclude from our preliminary studies that the front-end of the FNAL 8-GeV linac can successfully accelerate 100 mA beams. Operating the linac with a longitudinal to transverse emittance ratio of $\epsilon_L/\epsilon_T = 3$ instead of $\epsilon_L/\epsilon_T = 2$ is favorable in terms of emittance growth. A real machine should have more thorough analysis.

VI. CONCLUSION

A SC front-end presents a competitive option for high-intensity ion linacs, not only in terms of power consumption but also to ensure high-quality beams. The front-end of the FNAL 8-GeV linac accelerates beams from the Ion Source up to 420 MeV using CH cavities to ~10 MeV followed by SC spoke (SSRs and TSRs) resonators. All operate at the 4th sub-harmonic of the ILC frequency. The use of SC solenoids results in a compact lattice below ~120 MeV and facilitates the use of the high accelerating gradients offered by the SSR cavities. Also SC solenoids help mitigate halo formation and beam losses. The studies presented in this paper show an excellent behavior of the linac in terms of emittance growth and beam losses for the current design of the linac at 45 mA. An excellent agreement between the codes TRACK and ASTRA has also been observed. Preliminary studies showed that the FNAL 8-GeV linac front-end can be successfully applied to accelerate 100 mA beams.

Acknowledgments

The authors would like to thank K. Floettmann (DESY) for his support in using ASTRA, I. Hofmann (GSI) for providing the stability charts, V. Aseev and B. Mustapha (ANL) for helpfull discussion and information. This work is supported by the U.S. Department of Energy under Contracts DE-AC02-06CH11357 and DE-AC02-07CH11359.

[1] F. Gerigk, CERN-AB 2007-035, CERN, Geneva, Switzerland (2007).

[2] R. Pardo and G. Zinkann, in *Proceedings of the 9th Workshop on RF Superconductivity* (Santa Fe, New Mexico, 1999).

[3] C. Piel, K. Dunkel, F. Kremer, M. Pekeler, P. vom stein, D. Berkovits, and I. Mardor, in *Proceedings of the European Particle Accelerator Conference* (Genoa, Italy, 2008).

[4] B. Mustapha, P. N. Ostroumov, and J. A. Nolen, in *Proceedings of the Particle Accelerator Conference* (Albuquerque, New Mexico, 2007).

[5] J. L. Biarrotte, in *Proceedings of the International Linear Accelerator Conference* (Luebeck, Germany, 2004).

[6] A. Aleksandrov, C. Allen, S. Cousineau, V. Danilov, J. Galambos, D. Jeon, J. Holmes, T. Pelaia, M. Plum, A. Shishlo, et al., in *Proceedings of the European Particle Accelerator Conference* (Genoa, Italy, 2008).

[7] K. Hasegawa, in *Proceedings of the Particle Accelerator Conference* (Albuquerque, New Mexico, 2007).

[8] Tech. Rep. (2006), CERN-2006-006.

[9] Tech. Rep. (2005), URL `http://protondriver.fnal.gov/\#{}Technical\_Design\_Link`.

[10] P. N. Ostroumov, New Journal of Physics **8**, 281 (2006).

[11] M. Kelly, in *Proceedings of the International Linear Accelerator Conference* (Knoxville, Tennessee, 2006).

[12] K. W. Shepard, P. N. Ostroumov, and J. R. Delayen, Phys. Rev. ST Accel. Beams **6**, 080101 (2003).
[13] R. L. Madrak and D. Wildman, in *Proceedings of the International Linear Accelerator Conference* (Vancouver, British Columbia, 2008).
[14] R. W. Garnett, T. P. Wangler, F. L. Frawczyk, J. P. Kelley, and K. R. Crandall, in *Proceedings of the Particle Accelerator Conference* (Chicago, Illinois, 2001).
[15] D. Jeon, in *Proceedings of the Particle Accelerator Conference* (Portland, Oregon, 2003).
[16] B. I. Bondarev, V. V. Kushin, B. P. Murin, L. Yu, and A. P. Fedotov, Atomnaya Energiya **34**, 131 (1973).
[17] M. Marchetto, A. Bylinskii, and R. E. Laxdal (Knoxville, Tennessee, 2006).
[18] Z. Li, R. Tiede, U. Ratzinger, H. Podlech, C. Clemente, K. Dermati, W. Barth, and L. Groening, in *Proceedings of the International Linear Accelerator Conference* (Luebeck, Germany, 2004).
[19] P. M. Lapostolle, IEEE Trans. Nucl. Sci. **18**, 1101 (1971).
[20] V. N. Aseev, P. N. Ostroumov, and B. Mustapha, in *Proceedings of the Particle Accelerator Conference* (Knoxville, Tennessee, 2005).
[21] K. Floettmann, *ASTRA User Manual* (2002), URL `http://www.desy.de/\~{}mpyflo/Astra\_dokumentation`.
[22] P. N. Ostroumov, V. N. Aseev, and A. A. Kolomiets, Journal of Instrumentation **1**, P04002 (2006).
[23] G. P. Lawrence and T. P. Wangler, in *Proceedings of the Particle Accelerator Conference* (Vancouver, B.C., Canada, 1997).
[24] A. V. Fedotov, NIM A **557**, 216 (2006).
[25] I. Hofmann, G. Franchetti, J. Qiang, R. Ryne, F. Gerigk, D. Jeon, and N. Pichoff, in *Proceedings of the European Particle Accelerator Conference* (Paris, France, 2002).
[26] T. P. Wangler, in *Proceedings of the International Linear Accelerator Conference* (Monterey, California, 2000).
[27] I. Hofmann, Phys. Rev. E **57**, 4713 (1998).
[28] P. N. Ostroumov, B. Mustapha, and V. N. Aseev, in *Proceedings of the International Linear Accelerator Conference* (Nashville, Tennessee, 2006).
[29] F. Gerigk, in *Proceedings of the Joint USPAS-CAS-Japan-Russia Accelerator School* (Long Beach, California, 2002).
[30] L. M. Young, in *Proceedings of the Particle Accelerator Conference* (Chicago, Illinois, 2001).
[31] M. Reiser, *Theory and design of charged particle beams* (John Wiley & Sons, New-York, 1994).